Sliding wear of medium-carbon bainitic/martensitic/austenitic steel treated by short-term low-temperature austempering

LUO, Quanshun <http://orcid.org/0000-0003-4102-2129>, LI, Jianbin, YAN, Qintai, LI, Wenbo, GAO, Yubi, KITCHEN, Matthew, BOWEN, Leon, FARMILO, Nick <http://orcid.org/0000-0001-5311-590X> and DING, Yutain

Oral presentation & publication in 23rd International Conference on Wear of Materials, 26-28 April 2021
1st submission: 31st August 2020; Revised version: 25th December 2020; Accepted 19th January 2021

Sliding wear of medium-carbon bainitic/martensitic/austenitic steel treated by short-term low-temperature austempering

Quanshun Luo[1*], Jianbin Li[2], Qintai Yan[2], Wenbo Li[3], Yubi Gao[4], Matthew Kitchen[1], Leon Bowen[5], Nicholas Farmilo[1], Yutian Ding[4]

[1] Materials and Engineering Research Institute, Sheffield Hallam University, Sheffield, UK.
[2]China Railway High-Tech Industry Corporation Limited, Beijing, China.
[3]China Railway Baoji Bridge Group Co., Ltd, Baoji, Shaanxi Province, China.
[4] State Key Laboratory of Advanced Processing and Recycling of Nonferrous Metals, Lanzhou University of Technology, Lanzhou, Gansu Province, 730050, China.
[5] Department of Physics, Durham University, Durham, DH1 3LE, UK.
*Corresponding author: Dr Quanshun Luo, email: q.luo@shu.ac.uk, telephone 0044 114 2253649, mobile 0044 7967302493

Abstract

A medium-carbon Si-Mn-Ni-Cr-Mo alloyed (300M) steel was austempered for various short periods at its martensite-starting temperature of 285°C to seek improved sliding wear resistance as compared to the traditional martensitic and bainitic steels. Reciprocating sliding wear tests were performed against a WC/Co ball counterpart at a constant load of 50 N. The samples were characterised using field emission SEM, XRD and hardness testing. The associated wear mechanisms were analysed using SEM and cross-sectional TEM. The results revealed that a short austempering time of 6 minutes produced refined arrays of initial nano-bainitic ferrite laths and inter-lath filmy austenite and the majority martensite and retained austenite, while the majority of the microstructure remained martensitic with retained austenite. The hardness was unchanged to that of the as-quenched martensite of 6.4 GPa. Simultaneously the wear coefficient decreased by 41% from 2.67 to 1.58×10^{-15} $m^3N^{-1}m^{-1}$, which is also superior to both the tempered martensite at 1.65×10^{-15} $m^3N^{-1}m^{-1}$ and the lower bainite at 1.87×10^{-15} $m^3N^{-1}m^{-1}$. Increasing the austempering time to 20 and 60 minutes resulted in wear coefficients of 1.38 and 2.18×10^{-15} $m^3N^{-1}m^{-1}$, respectively. The improved wear resistance has been explained by the wear induced microstructure evolution, especially the carbon partitioning induced stabilisation of retained austenite. The high-stress sliding wear was found to be dominated by severe shear deformation, which resulted in a nano-laminate structured top layer. Delamination wear was found to take place within the embrittled nano-laminates.

Keywords: Nano-bainitic steel; Sliding wear; Short-term austempering; Cross-sectional TEM

1 Introduction

Wear resistant steels are widely used to produce railway crossings, loader buckets in mining industry, disc cutters of tunnel boring machines and many other components which withstand severe and complicated loads [1-4]. Most of these steels are classified as medium-carbon and multi-alloyed steels. The medium carbon content is selected to ensure combined strength and toughness properties whereas the multi-alloying aims to facilitate the formation of martensitic microstructure after targeted heat treatments. The mostly recognised wear mechanisms under the applications mentioned above include various severity of plastic deformation and fatigue, spalling, abrasion, and delamination. The theory of delamination wear was first introduced by Suh in 1970's [5]. Repeated or cyclic contact loads lead to dislocation pile-up, subsurface voids, crack nucleation, and eventually the generation of thin delamination sheets. In the follow-up studies, the delamination theory was detailed to include progressive accumulation of plastic shear deformation. Greiner et al reported that early plastic deformation could occur after only a few cycles of reciprocating sliding [6]. It has been often reported that wear induced deformation was featured by extremely fine-grained structure, nano-grained laminates, and white-etching layers (WEL) [3, 7-8]. Shear deformation was found as a predominant factor of various wear failures in many circumstances, such as disc cutters made of tool steel AISI H13 in cutting various rocks, the abrasive wear of various alloy steels, scrap shear blades and ball mill liners made from martensitic and pearlitic steels, as well as martensitic bearing steels [2,4,9].

For wear resistant steels, heat treatment is the final stage of strengthening and hardening to optimise its microstructure and wear resistance. Traditionally, the most common hardened microstructure for wear resistance includes tempered martensite produced by quenching and tempering (Q-T) treatments and lower bainite by austempering at a constant transformation temperature. Bainitic steels were reported to have increased wear resistance when compared to those with martensitic, pearlitic and ferritic microstructures [1,10].

In recent years, fundamental research on austenite transformation mechanisms has promoted innovation in heat treatment processes, such as the improved understanding of carbon partitioning and the subsequent invention of quenching-partitioning (Q-P) heat treatment and quenching-partitioning-tempering (Q-P-T) [11,12]. In these new treatments, carbon partitioning resulted in increased amount of stabilised retained austenite (RA) and consequently strengthened the

resistance against delamination wear [12-14]. For bainitic steels, lowering the isothermal transformation temperature leads to finer bainitic laths and, in some specially designed high-carbon Si-Mn-Cr alloyed steels, prohibits carbide precipitation. Such nano-bainitic structures have been found to show remarkably lower wear rates [15,16].

A short-term and low-temperature austempering heat treatment has been developed recently [17]. In the new treatment, undercooled austenite firstly undergoes isothermal transformation in a limited time to form nano-width bainitic ferrite (BF) and then, in the subsequent cooling, transforms to martensite. The resultant multiple structure of BF, martensite and RA shows similarly high hardness and strength properties while maintaining more RA than the quenched martensitic structure. The related strengthening mechanisms matches those proposed by other researchers [18], i.e. enhanced hardening of martensite by bainite transformation induced carbon partitioning, strain hardening of bainite due to volume expansion accompanying the subsequent martensite formation, as well as the pre-bainite formation induced structural refinement. In addition, the new process is of much lower production cost owing to the substantially shortened isothermal bathing time. The aim of the present work is to investigate the high-stress sliding wear property of medium-carbon alloyed steels after short-term low-temperature austempering treatments. The microstructure evolution with increasing austempering time has also been studied along with comprehensive analysis of the wear mechanisms. We expect to obtain better wear resistance than the conventionally hardened steel.

2 Experimental methods

The sample material was a medium-carbon multi-alloyed 300M steel, which was provided as a hot-rolled and annealed bar having chemical composition (in wt%) of C 0.42, Mn 0.75, Si 1.65, Ni 1.80, Cr 0.80, Mo 0.40, V 0.07, and Fe in balance. Its Ms (martensite-starting temperature) and lower bainite transformation temperature are 285°C and 320°C, respectively [19]. The samples were cut to 8 mm long coupons with a 30 mm diameter. Three electrical furnaces were used for the heat treatments, one for austenizing heating and holding at 900°C and other two being pre-heated at 285°C and 320°C, respectively, for the designed austempering treatments. The treatment parameters are summarised in Table 1, where samples TM and LB stand for the tempered martensite and lower bainite, respectively. The heat treated coupons were sectioned as 25 × 8 × 6 mm^3 cuboid blocks and having the 25 × 8 mm^2 section for the testing and analyses. Each sectioned sample was thermal mounted in Bakelite (at 350 MPa pressure and 120°C - 140°C for 4 minutes), then ground and polished to scratch-free mirror polishing. The metallographic polishing was conducted with 6-μm diamond slurry and then with 1-μm diamond slurry. All the tests and characterisations were carried out on the Bakelite-mounted samples. For the microscopic observations of microstructure, the metallographically polished samples were etched using 2% nital.

Table 1 Heat treatment parameters and hardness property

I.D.	**Heat treatment***	**HV_{30}, GPa**
M	Water quenching	6.37 ± 0.03
TM	Water quenching, 200° / 120 min tempering	6.15 ± 0.03
BM-6	285° / 6 min austempering	6.38 ± 0.03
BM-20	285° / 20 min austempering	5.90 ± 0.03
BM-60	285° / 60 min austempering	5.51 ± 0.02
LB	320°C / 20 min austempering	5.43 ± 0.11

*The austenisation of all the samples was heating to 900°C and holding for 30 minutes.

The Vickers' hardness was measured at 30 kg load on a Struers Duramin-40 AC3 hardness tester. Five indents were made on each sample to obtain the average hardness value and standard deviation.

A CERT-UMT-2 multi-functional tribometer was employed to perform ball-on-disc reciprocating sliding wear tests against a WC ball (HV 15.5 GPa) counterpart which had a polished surface and a diameter of 6 mm. Prior to each test, the applied WC ball was cleaned in acetone and then fixed to the ball holder ensuring that the polished spherical part, instead of previous wear induced flat facet, was used to make a new sliding test. The wear tests were conducted at an applied normal load of 49 N, with a reciprocating sliding length of 8 mm and a frequency of 23.5 Hz. The initial ball-flat contact was estimated to have the maximum compressive stress of 2.912 GPa, which did not represent the conformal sliding wear due to the occurrence of severe plastic deformation. The testing sequence for each sample included a 40-minute running-in period, corresponding to 1,880 reciprocating sliding passes and a sliding distance of 15.04 m. The resultant wear scars of the flat sample and the ball were measured by the method described below. The sample and ball were then reloaded into the same position to run the conformal sliding wear for 360 minutes, corresponding to 16,920 reciprocating sliding passes and a sliding distance of 135.36 m. One sliding wear test was made on each sample under the defined procedure and conditions.

After each wear test, the obtained 8-mm long wear scar of the flat sample and wear crater on the ball were measured using the 3D micrometer stage of the Struers Duramin-40 AC3 hardness tester. The former included three cross-scar linear profiles in the middle 2-mm period of the 8-mm wear scar, at a spatial resolution of 0.1 μm, whereas the later included diameters both parallel and perpendicular to the sliding traces. The measurements were adopted to calculate the volume wear and wear coefficient (i.e., volume wear at unit applied load and unit sliding distance, $m^3 \cdot N^{-1} \cdot m^{-1}$). The average ball-to-flat contact pressure was estimated to be 277 and 112 MPa according to the diameter measurements of the ball wear craters, prior to and after the 360-minute wear test, respectively.

An Empyrean X-ray diffractometer was employed to characterise the crystallographic structure of the hardened samples, using a filtered Co radiation at a wavelength of 0.1789 nm ($K_{\alpha 1}$-Co). Each diffraction curve was acquired at a step size 0.026° and a slow scan speed $0.0022° \cdot s^{-1}$. The volume fractions and carbon contents of the ferrite and austenite phases were calculated using the methods published in our previous research [17]. A FEI Nova200 field emission scanning electron microscope (SEM) was employed for microstructure observation and worn surface analysis. The latter included direct observation of the as-obtained wear scars and the preparation of longitudinal cross-sections of selected wear scars to examine the microstructure evolution from the bulk to the top worn surface. Cross-sections of selected wear scars were also observed by transmission electron microscopy (TEM) using a field-emission JEOL 3100F TEM operating at 200 kV. Cross-sectional TEM thin foils were prepared using low-angle ion-milling method following the procedure described in previous publication [20]. In brief, a thin longitudinal cross-section of an obtained wear scar, approximately 2.5 mm in length and 1.0 mm in thickness, was cut using a 0.45 mm thick SiC abrasive cutting wheel under water-based cooling. The thin specimen was mounted on a glass plate using thermal wax and then manually thinned from both sides to a thickness of 30 - 50 μm by metallographic grinding and polishing. After cleaning in acetone, the thinned specimen was mounted in a TEM sample grid (pure copper, 3.05 mm in diameter, having a slot hole of 2.0 mm in length and 1.0 mm in width) using epoxy resin. The final thinning was made using a Gatan 691 Precise Ion Polishing System.

3 Results and discussion

3.1 The hardness and wear properties

Table 1 has listed the hardness property of various heat treated samples. Sample M shows a hardness value of 6.37 GPa, which represents the highest hardness of the steel achieved by water-quenching to the martensitic microstructure. Sample BM-6 shows a hardness of 6.38 GPa, slightly higher than Sample M. The austempering time of 6 minutes was chosen in this work after our preliminary experiments which showed a peak hardness when the austempering time was between 6 and 10 minutes. The high hardness value confirms the strengthening resulting from the short-term austempering treatment, which is consistent to our previous work on another ultrahigh strength steel 56NiCrMoV7 as well as the findings of other researchers [17, 18, 21]. Further increase of austempering time to 20 and 60 minutes resulted in lower hardness values of 5.90 and 5.51 GPa, respectively. Comparison of the BM-20 and LB samples indicates that higher austempering temperature leads to lower hardness, which is in agreement with the results published in the literature [10].

Figures 1a and 1b show the friction coefficient curves and the measured line profiles of the obtained wear scars, respectively. The calculated wear coefficients as well as the average friction coefficients are summarised in Figure 2. Figure 1a indicates that in each sliding process, the friction coefficient experienced a period of dynamic running-in and eventually reached steady-state. The average values of friction coefficients fall in a range of 0.55 - 0.60, Figure 2. In Figure 1b, the line profiles exhibit good repeatability. The wear coefficients of all the tested steel samples fall in the scale of 10^{-15} $m^3N^{-1}m^{-1}$, whereas Sample M exhibits the highest wear coefficient of 2.67×10^{-15} $m^3N^{-1}m^{-1}$. Samples BM-6 and BM-20 show slightly smaller wear scar sections, both have lower coefficient than the as-quenched sample, being 1.58 and 1.38×10^{-15} $m^3N^{-1}m^{-1}$, respectively. These values are lower than the coefficients of the tempered martensite (TM) and lower bainite (LB). The results also indicate that longer austempering time, e.g., 60 minutes in this case, is not recommended for the substantially increased wear coefficient of 2.18×10^{-15} $m^3N^{-1}m^{-1}$. The WC balls exhibited wear coefficients comparable to each other in the order of 10^{-15} $m^3N^{-1}m^{-1}$. An exception might be noticed where the ball wear caused by Sample TM is substantially higher than those caused by other samples, however further analysis was not undertaken to explain this phenomenon.

3.2 The microstructure characteristics

Figure 3 shows SEM observations of the microstructure evolution with increasing austempering time. Sample BM-6 shows primarily microstructure of martensite and RA, similar to the as-quenched microstructure of Samples M and TM, comparing Figures 3a, 3d and 3e. Such morphology of martensitic microstructure has been frequently observed in our previous research [17]. In addition, Sample BM-6 also shows a small amount of initial BF laths which exhibit non-uniform distribution, preferentially grown from prior austenite grain boundaries, Figure 3a. The preferential distribution

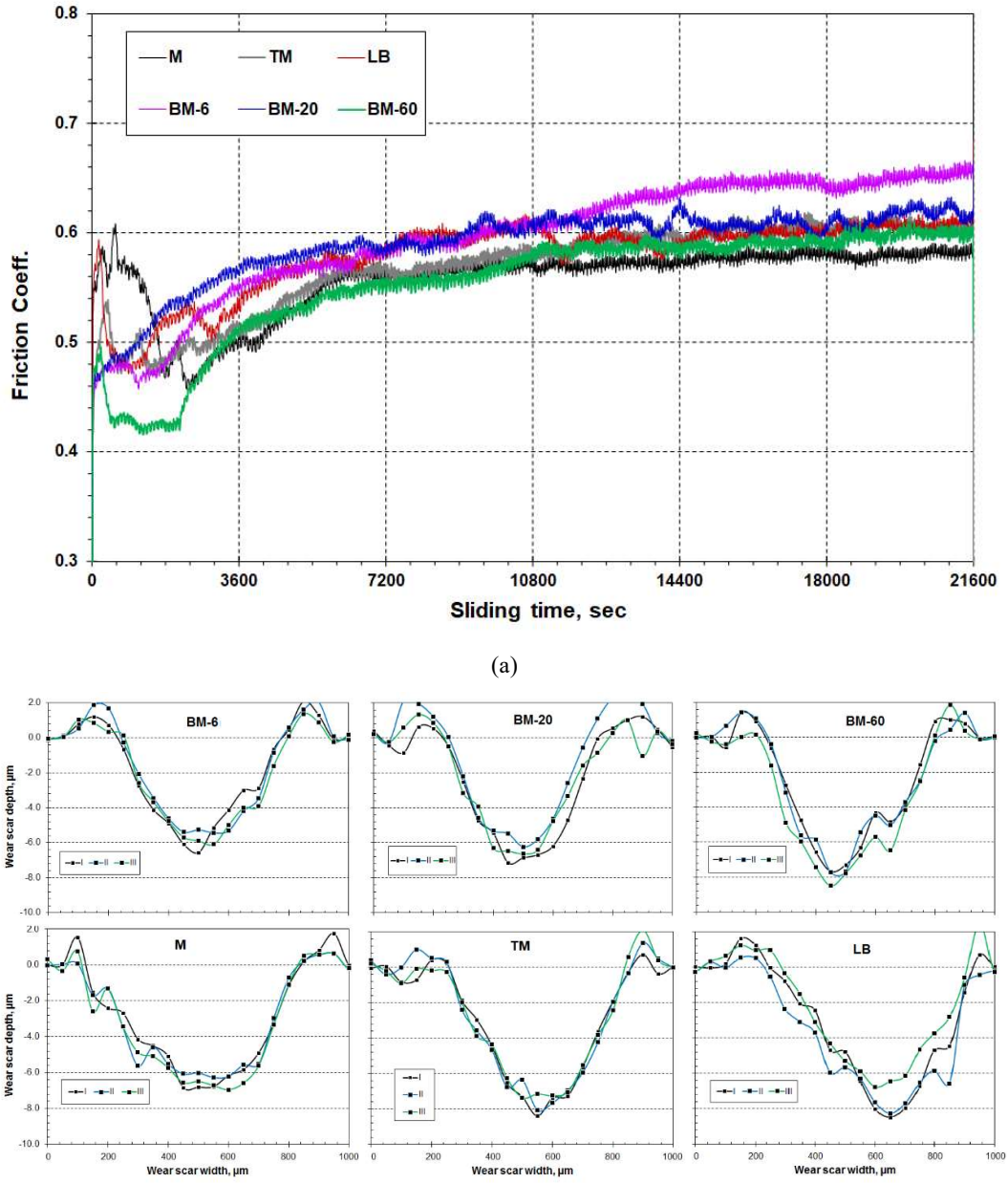

Figure 1 Experimental measurements of the sliding wear tests: (a) The coefficients of friction plotted versus siding time; and (b) Line profiles of the wear scars after 400 minutes of reciprocating sliding wear.

provides evidence to the kinetics of bainite transformation where autocatalytic nucleation of BF occurs preferentially in the austenite grain boundaries [22, 23]. The widths of the BF laths and the inter-lath filmy austenite were measured to be 110 ± 37 nm and 48 ± 5 nm, respectively. The BF structures in the low-temperature austempered samples (BM-6, BM-20 and BM-60) were significantly refined as compared to the lower bainite (Figure 3f). Such refining was attributed to the low transformation temperature, which has been reported by other researchers in the studies of nanobainite steels [15].

The BF and RA becomes the major structural constituent when the austempering time was increased to 20 minute, Figure 3b. The martensitic regions are intersected by fine BF arrays. Such partitioning of prior austenite grains has already been observed in the 6 minute austempered sample and is important experimental evidence of prior bainite transformation induced grain refining as proposed previously by Tomita [24]. The microstructure of Sample BM-60 is almost full of mixed BF and RA, whereas martensite-like morphology (seeing Figure 3d) has completely disappeared.

Figure 4 shows XRD patterns of samples, which exhibits clear presence of bainitic/martensitic ferrite and RA. Note that the austempered samples BM-6, BM-20 and BM-60 show increased peak intensities of austenite as compared to the as-quenched sample M, e.g., the A(200) peaks. The austenite peaks of Sample LB shift to lower diffraction angles, suggesting

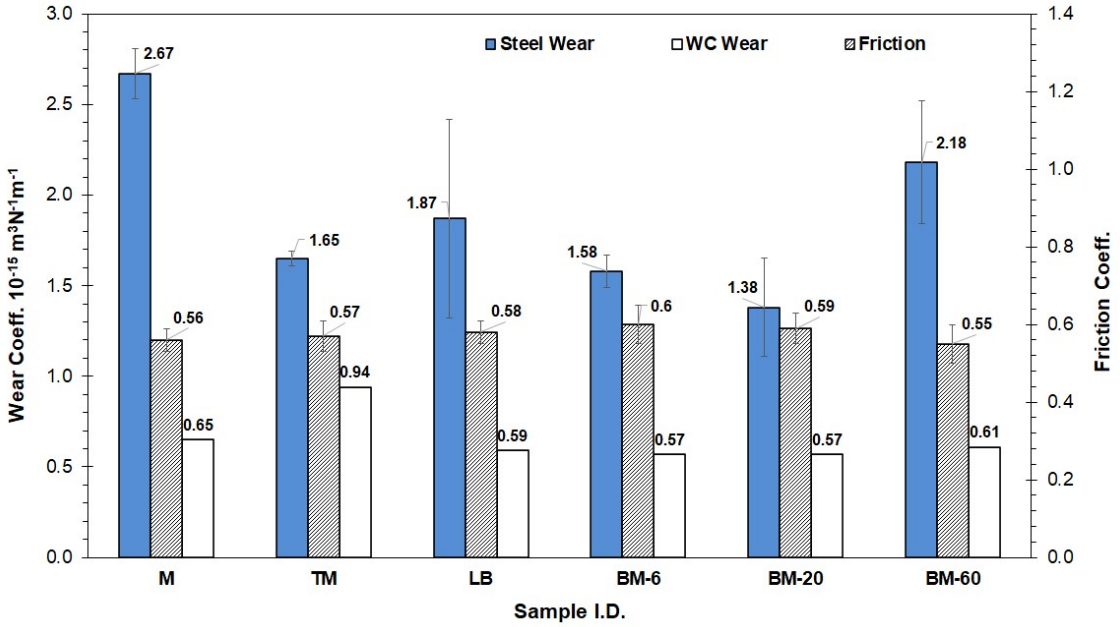

Figure 2 The wear coefficients of the flat and ball samples and the average coefficient of friction.

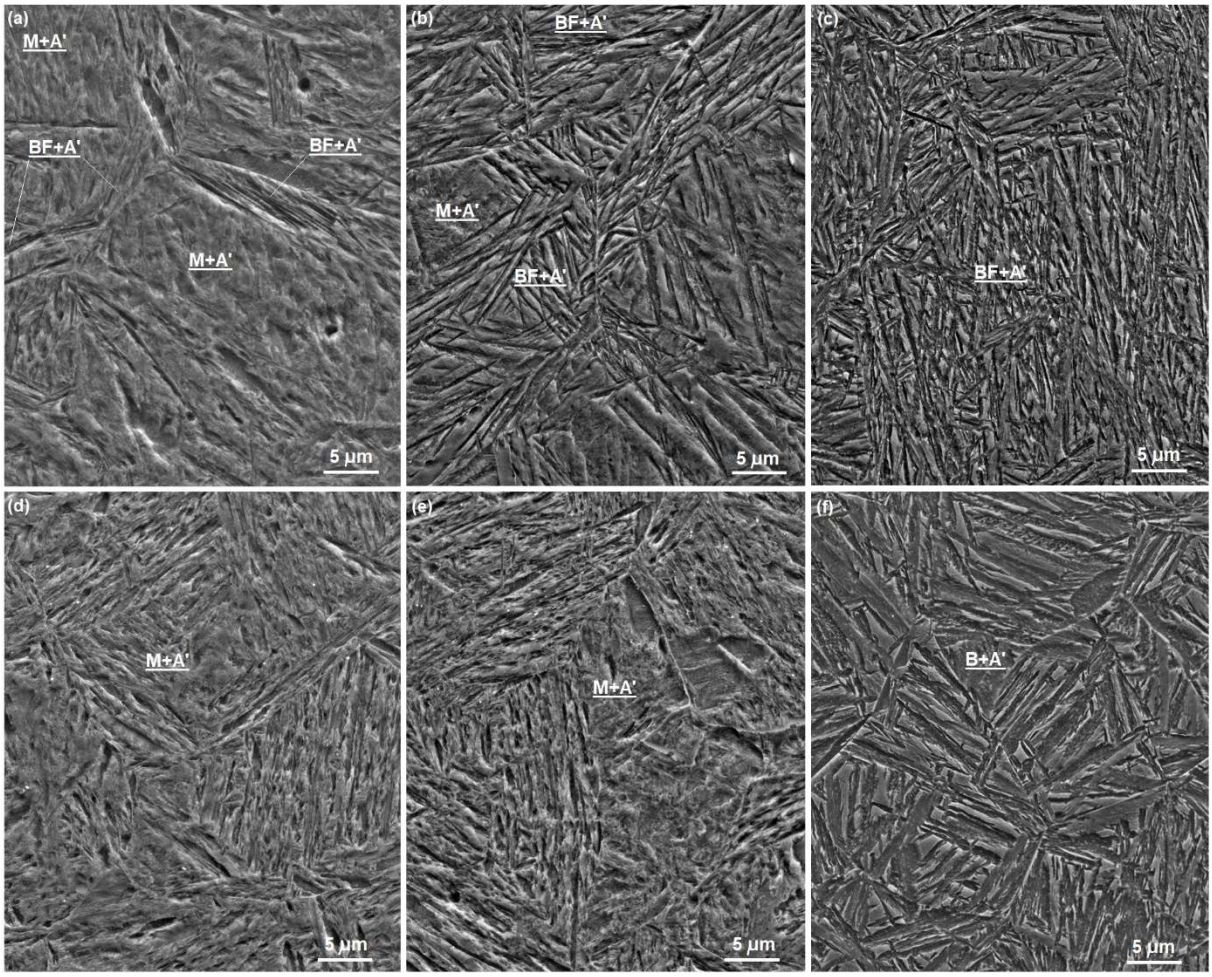

Figure 3 Microstructure of samples: (a) BM-6; (b) BM-20; (c) BM-60; (d) M; (e) TM; and (f) LB.

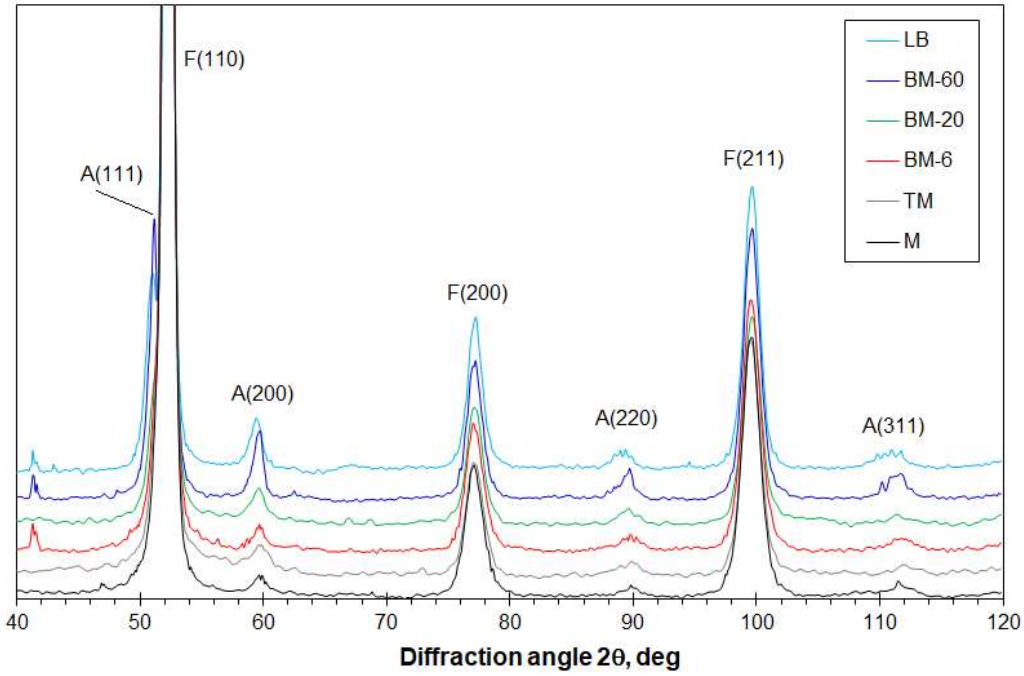

Figure 4 XRD patterns of the austempered and as-quenched samples.

Table 2 Quantified XRD results: the volume fraction (V_γ) and carbon content (C_γ) of retained austenite, and the micro-strains of retained austenite (ε_γ) and M/B ferrite (ε_α).

Sample ID	Measured values, %				Normalised to martensitic steel, %			
	V_γ	C_γ	ε_α	ε_γ	V_γ	C_γ	ε_α	ε_γ
M	3.8 ± 1.0	0.78 ± 0.12	0.77	0.73	100	100	100	100
MB-6	4.2 ± 1.4	0.9 ± 0.12	0.73	0.75	111	115	95	103
MB-20	6.4 ± 0.6	1.02 ± 0.06	0.70	0.80	168	131	91	110
MB-60	11.9 ± 1.3	1.02 ± 0.09	0.67	0.67	313	131	87	92
LB	9.2 ± 0.5	1.30 ± 0.08	0.64	0.84	242	167	83	115

expanded lattice due to more enriched carbon. Table 2 presents the results of quantitative analyses out of the XRD patterns. Sample M is shown to contain a small fraction (3.8%) of RA. Its higher carbon content (0.78%) than the average carbon content of the steel (0.42%) was attributed to the carbon partitioning. The austempered samples show increased fraction and carbon content of retained austenite with increasing austempering time, while the carbon content became stabilised at 1.02% when the austempering time was longer than 20 minutes. These results denote enhanced carbon partitioning in the austempering treatment. The increases in fraction and carbon content of the RA are expected to favour the TRIP (transformation induced plasticity) effect in sliding wear [16].

Sample M exhibits the highest ε_α value of 0.77%, whereas the austempered samples gradually lower ε_α value from 0.73% to 0.67% following the increased austempered time. The primary phase associated with this sample is martensite/bainitic ferrite, the strengthening is therefore governed by the hardness property, shown in Table 1. Moreover, one may consider the co-existing bainitic and martensitic ferrites and the fact that the BF was formed prior to the martensitic ferrite. The role of carbon partitioning in the austempering was re-distributing carbon between the newly growing BF and its parent austenite phase. Enriched carbon and increased amount of austenite imply increased carbon depletion of the BF phase in the austempered samples. Therefore, it is believed that the decreased lattice strain of the ferrite should be preferentially allocated to BF. In contrast to the BF, the martensitic ferrite could have encountered more lattice strain due to the increased carbon content. This increased straining is indirectly demonstrated in the increased RA straining. In Samples BM-6 and BM-20, the ε_γ values are 0.75 and 0.80%, indicating 3% and 10% increases over Sample M, respectively. It is believed that the increased straining was attributed to the volume expansion of newly formed martensite, whereas the scale of volume expansion is known to be proportional to its tetragonal ratio or carbon content. Therefore, the quantitative XRD

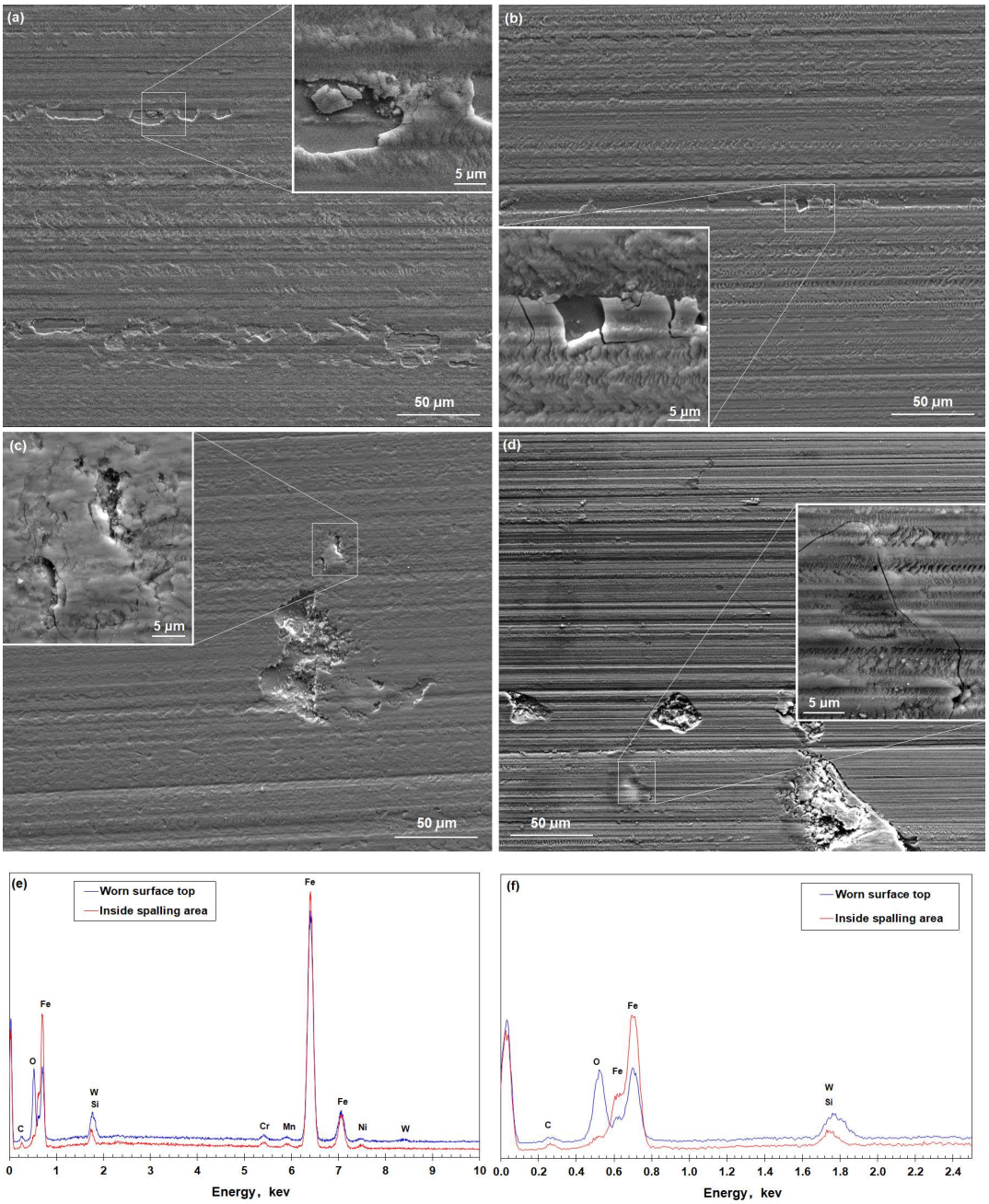

Figure 5 SEM observations and EDX analyses of worn surfaces after 400 minutes (18,800 passes) of reciprocating sliding: (a) Sample M; (b) Sample BM-6; (c) Sample BM-20; (d) Sample BM-60; (e) a comparison of the EDX spectra acquired in different areas; and (f) the same spectra as shown in (e) to be displayed at a higher energy resolution.

analyses, Table 2, shows evidence of the enhanced hardening of the martensitic ferrite, which is consistent with the proposed strengthening mechanisms of multiphase martensite-bainite-austenite microstructure [18, 24].

3.3 The wear mechanism analyses

3.3.1 SEM observation of worn surfaces

Selected SEM observations of worn scars are presented in Figure 5. At low magnification, the worn surfaces are full of sliding induced grooves and fish-sale patterns. The sliding grooves are more pronounced in the BM-60 worn surface, which should be attributed to its lower hardness. The fish scales are typical features of self-mating adhesive sliding contact. In literature, such patterns were described as a sequence of densely packed and or sintered tribofilm after powdering, self-agglomerating and adhering wear debris [25, 26]. In previous studies it was found that in the dry sliding wear of transition

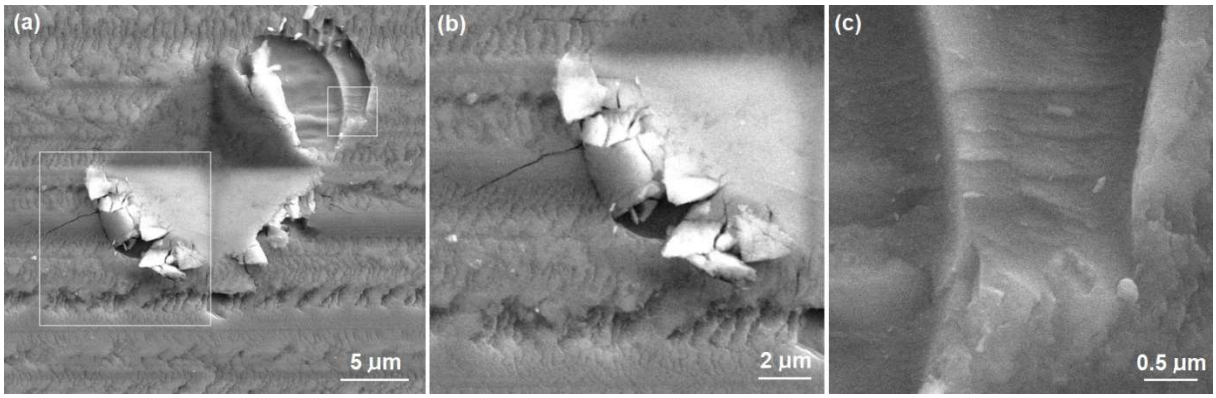

Figure 6 SEM observations of indention induced cracking and spalling in the top worn surface: (a) overview of the indent and failure; (b) the cracking and fragments; and (c) the spalling scar.

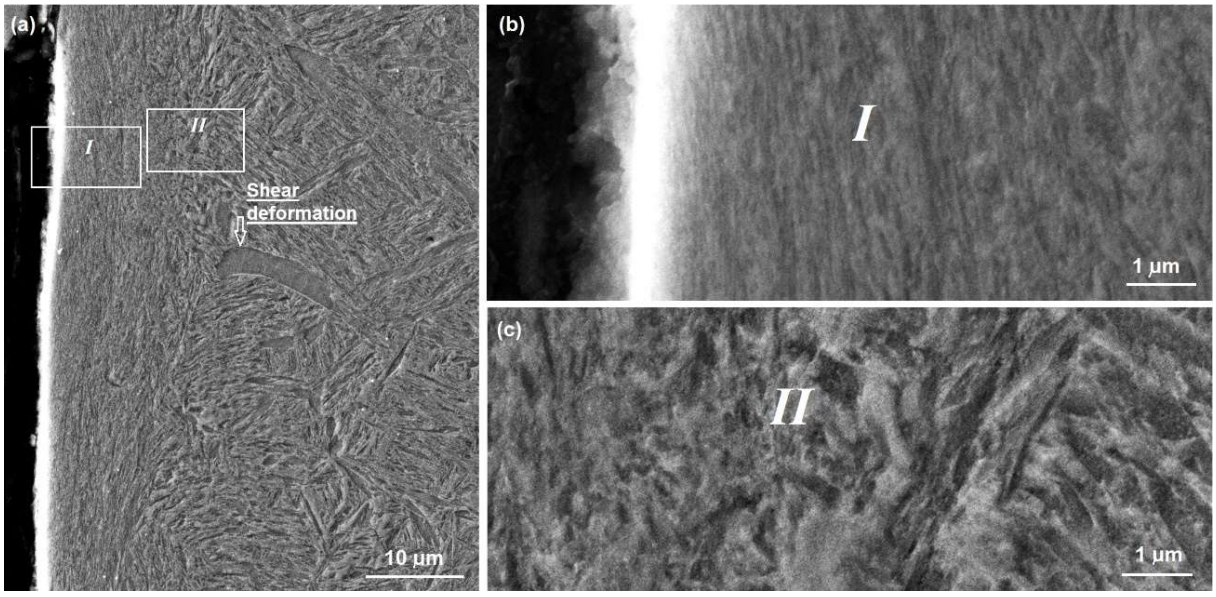

Figure 7 SEM images on a wear scar cross-section (Sample BM-6): (a) overview of subsurface microstructure evolution; (b) wear induced nano-laminate structure in a depth of 8µm; and (c) the transition from plastically deformed structure to the regular non-deformed structure at the depth of 11µm.

metal nitride coatings that such worn surface roughening due to fish-scales, triggered high frictional forces [27]. On the other hand, a smooth glaze layer on worn surface prevented the formation of such fish-scale roughening and led to self-lubrication [28]. The inserts in Figure 5 show wear induced cracking and spalling failures. The inserts reveal that spalling failures took place within very small depths and generated delamination sheets, whereas nano-scale powders could be generated from the edges of the fish-scales.

It is suspected that cracking and spalling failures in such small depths were caused by sliding induced strain-hardening resulting in embrittlement, and residual stresses. Vickers hardness indentations were applied to selected worn surfaces to confirm this. Typical SEM observation are shown in Figure 6. In Figure 6a, the indent edges in the lower part shows fragments and radial cracks. More details of the fragments and cracking are shown in Figure 6b, which show the brittle nature of the worn surface. A large spalling pit was formed outside the edge of the upper part of the indent, Figure 6a. A small area of the spalling pit is enlarged in Figure 6c, which indicates features of brittle cracking and fracture. In addition, the rough bottom of the spalling pit suggests deformation induced surface grooving or roughening, implying subsurface deformation. So far, the SEM observations indicate that it was the repeated plastic deformation which resulted in the spalling or delamination wear as a sequence of worn surface hardening and embrittlement as well as residual compressive stresses. The reciprocating sliding also caused oxidation of the wear debris and top worn surface.

3.3.2 Cross-sectional SEM and TEM observations of wear induced microstructure evolution

Figure 7 shows the profile of wear induced plastic deformation beneath the worn surface of Sample BM-6. In Figure 7a, the outmost worn surface exhibits a layer of extremely fine lamina microstructure to a depth of approximately 12 µm. There is no distinct interface between the deformed and un-deformed areas. Instead, the straining scale varies in a gradient

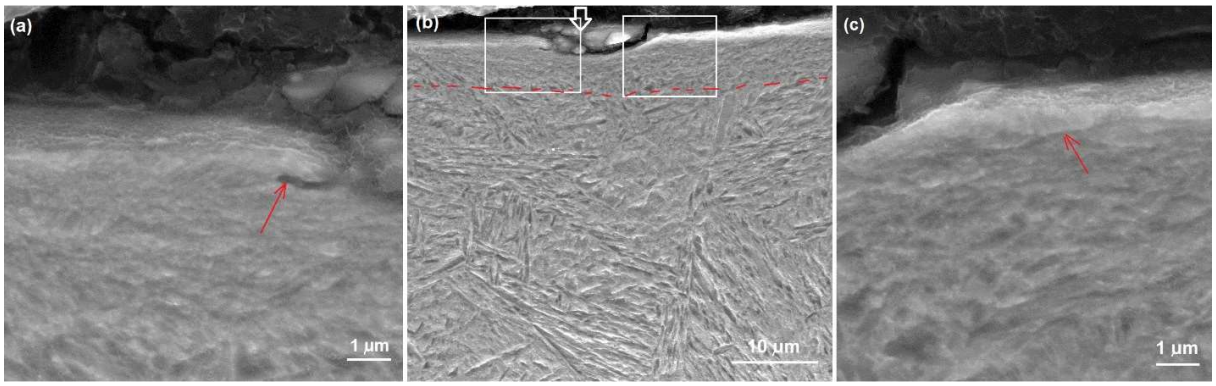

Figure 8 SEM images of the wear scar longitudinal cross-section of Sample BM-6 showing a small spalling pit inside the depth of nano-laminates: (b) the spalling pit on the top; (a, c) details of the nano-laminates and subsurface cracking.

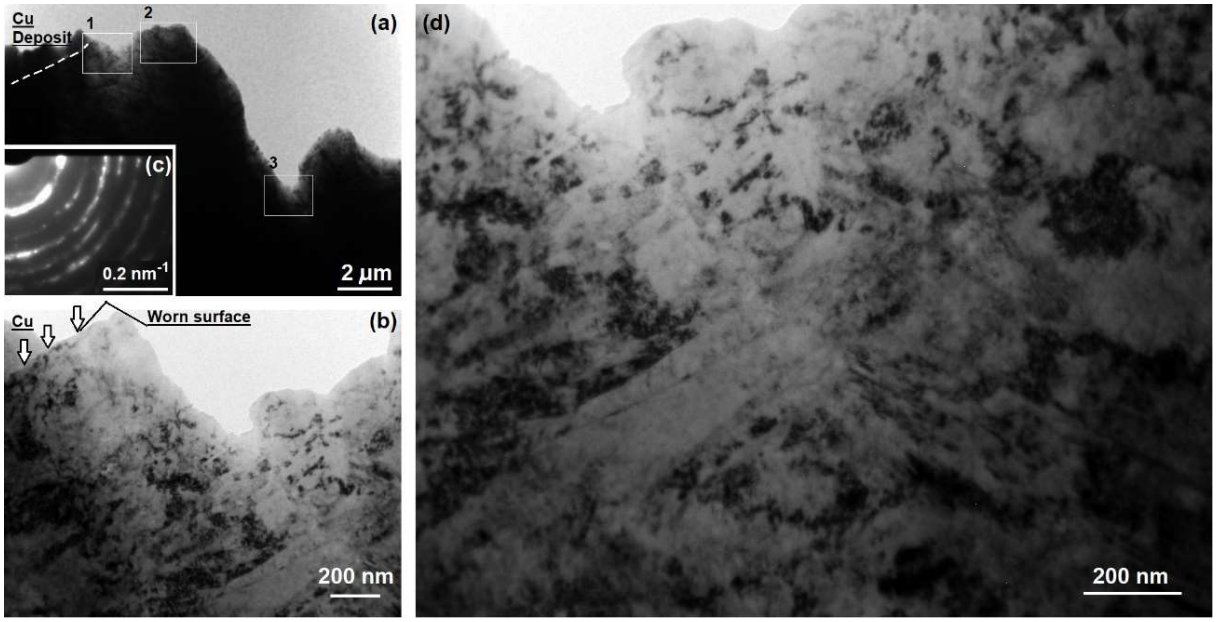

Figure 9 TEM images of the wear scar longitudinal cross-section of Sample BM-6r: (a) a low-magnification view of the cross-sectional foil sample; (b) a BF image of Zone 1 showing the worn surface top; (c) a selected area electron diffraction pattern taken from Zone 1; and (d) an enlarged image of Zone 1 showing nano-laminates.

from bulk to the worn surface. Shear deformation was clearly observed in this image, as indicated by the arrow, where a thick bainite gain, approximately 25 μm from the surface appears to have bent following the shear deformation. The gradient deformation differs from those films of agglomerated and sintered wear debris as reported in literature, as those films showed a distinct interface to the worn surface [25, 26]. Figures 7b and 7c are high-magnification images taken from the outmost worn surface and the deformation-transition area, respectively, seeing the marked areas in Figure 7a. The fine laminates in the top 2.5 μm from the worn surface show individual laminate thickness of 75 ± 16 nm, as measured from Figure 7b and with increasing depth, the laminate gradually becomes coarser. In Figure 7c, the transition from the deformed fine structure to the regular un-deformed structure is progressive without a sharp interface. Such progressive depth-dependent plastic deformation has been reported repeatedly in literature [7, 9, 25, 28]. Thus, it can be concluded that the nano-laminates were produced by progressively accumulated plastic strain following the wear induced microstructure evolution as observed by cross-sectional SEM observations. An example is shown in Figure 8, where a spalling pit is imaged on the worn surface of Sample BM-6 exactly inside the depth of fine laminates. In the high-magnification images in Figures 8a and 8c, subsurface cracks were found, which seemed to undergo further propagation and may lead to more spalling or delaminating. No cracking or spalling phenomenon were found beyond the depth of fine laminates.

Figure 9 shows TEM observations of a longitudinal worn cross-section of Sample BM-6. In the low-magnification bright field (BF) image in Figure 9a, the areas marked Zone 1 and Zone 2 are in close vicinity of the worn surface, as guided by the white dish line. The top edge of the worn surface is beneath a copper deposit layer, which was formed by progressive deposition of sputtered copper (the TEM slot grid) in the ion-beam milling stage of the cross-sectional specimen thinning.

Both zones show deformation induced fine laminate microstructure. Zone 3 (at a depth of approximately 9 μm from the worn surface) shows very little evidence of deformation. The area of Zone 1 was observed at higher magnifications, Figures 9b and 9d. The top layer to a depth of 0.5 μm exhibits nano-scale features derived from the bright-field imaging mode (i.e., diffraction contrast) of random distribution, lacking the lamina morphology. Selected area electron diffraction analysis of that area exhibited strong ring patters indicating its polycrystalline microstructure, Figure 9c. In the depth range of between 0.5 μm and 1.2 μm the laminate structure could be observed. The thickness of the laminates has been measured from Figure 9d to range from 14 to 45 nm, or 28 ± 13 nm. The grains were found to become coarser at increasing depths from the worn surface. The TEM observations were consistent with the cross-sectional SEM results in the observed gradient profile of the wear induced deformation. Moreover, the TEM observation provide an important complementary view on the non-laminating structure of the top worn surface. The disappearing of nano-laminating morphology might be attributed to the combined shear and thermal effects in the close vicinity of the sliding surface since the friction induced flash heating might cause dynamic recovery of the highly strained structure.

Nevertheless, the cross-sectional electron microscopy confirms the generation of severely deformed laminating microstructure.

3.3.3 SEM and EDX analyses of wear debris

Figure 10 shows SEM observations of wear debris and a wear scar of the counterpart WC ball. Figure 10a shows the wear debris produced by 40 minute wear of Sample BM-20, which comprises thin flakes and fine powders. The large flakes, e.g. No. 3 - 6 as labelled, are either feature-less and smooth or show wrinkles, indicating repeated plastic deformation prior to their detaching from the worn surface. The fine powders have sizes ranging from sub-micron to micron scale. Figure 10b shows wear debris produced after 400 minutes of wear of the BM-20 sample. The flat surfaces of several flakes show fish-scales, which matches the SEM observation of the worn surfaces (to be shown later), indicating severe self-mating adhesive sliding of the worn surface. Some of the fine fragments show cross-sections, in which the thickness has been measured to be 0.8 - 1.0 μm for thick flakes and 0.2 - 0.3 μm, for thin sheets. The fine powders were measured to be 120 - 160 nm in diameter. Figure 10c shows more details of the fine fragments and thin flakes. The thickness of the thick and thin flakes has been measured to be 0.5 - 0.8 μm and 0.2 - 0.3 μm, respectively. SEM-EDX analysis was applied in the marked points or area in Figure 10a, seeing the selected results in Table 3. Related spectra are shown in Figure 10d. Major components of the wear debris include oxygen, iron, and tungsten, indicating wear of both parts. The presence of oxygen suggests that oxidation took place while the wear debris was engaged in the reciprocating sliding. Similar SEM-EDX results were obtained from the wear debris in the wear scars. In addition, the presence of W and Co in the wear debris was also noticed, although their quantities are smaller than Fe, indicating the wear of the WC counterpart.

3.3.4 SEM observation of the WC counterpart worn surface

Selected worn surfaces of the WC balls were also analysed using SEM. An example of the observations made on the WC ball, following 40 minutes of wear of the BM-20 sample, is shown in Figure 11. The worn surface is generally flat and smooth, having dispersed loose wear debris attached on the observed area, Figure 11a. Figure 11b is a view of the whole wear scar. Careful examination of the worn surface revealed parallel sliding grooves in the worn surface along with areas of transferred material. Some areas of transferred material are labelled by arrows in Figure 11a. All the observed WC grains, regardless of sizes and shapes, were embedded in the bulk without cracking or spalling. Figure 11c shows details of the transferred material, as highlighted in Figure 11a. The transferred material exhibits fish-scale patterns similar to those being observed on the worn surfaces (e.g., in the inserted high-magnification images in Figure 5). EDX spectra were acquired in areas of the transferred material, loose wear debris and on a clean area of WC worn surface, as summarised in Figures 11 d-e in two levels of energy resolution respectively. The clean WC worn surface was clearly free from Fe and O. The wear debris and transfer material both show Fe and O in addition to the strong spectroscopic peaks of W. In the interpretation, however, it should be pointed out that the detected W was predominantly from the WC worn surface for the transferred material layer was not thick enough to absorb the characteristic X-rays emitted from the WC beneath it. Nevertheless, the spectroscopic analysis clearly indicates Fe-O based wear debris and material transfer as compared to the clean WC free from Fe and O. As these transferred material attached strongly on the WC worn surface, these patterns confirm partial self-mating adhesive contact between a sliding pair of steel sample and the transferred material in addition to the sliding contact between the dissimilar surfaces.

4 Discussion

The new development of current austempering treatment has been both the short time and the low temperature, which allowed the prior bainitic transformation and subsequent martensite transformation to form a mixture of bainite (refined martensite and RA) and martensite (nano-scale BF laths separated by filmy austenite). The new treatment has several advantages. Firstly, the lowered transformation temperature made the resultant BF and RA even finer than lower bainite. The refinement is consistent with the literature regarding the formation of nano-bainite [15]. Secondly, the partitioning of prior austenite by the BF laths made the resultant martensite refined, whereas the carbon partitioning accompanying the BF growth make the martensite hardened due to the resultant carbon enrichment. The peak hardness and strength properties of bainite-martensite mixture were reported in literature [18, 24], while our experimental findings have

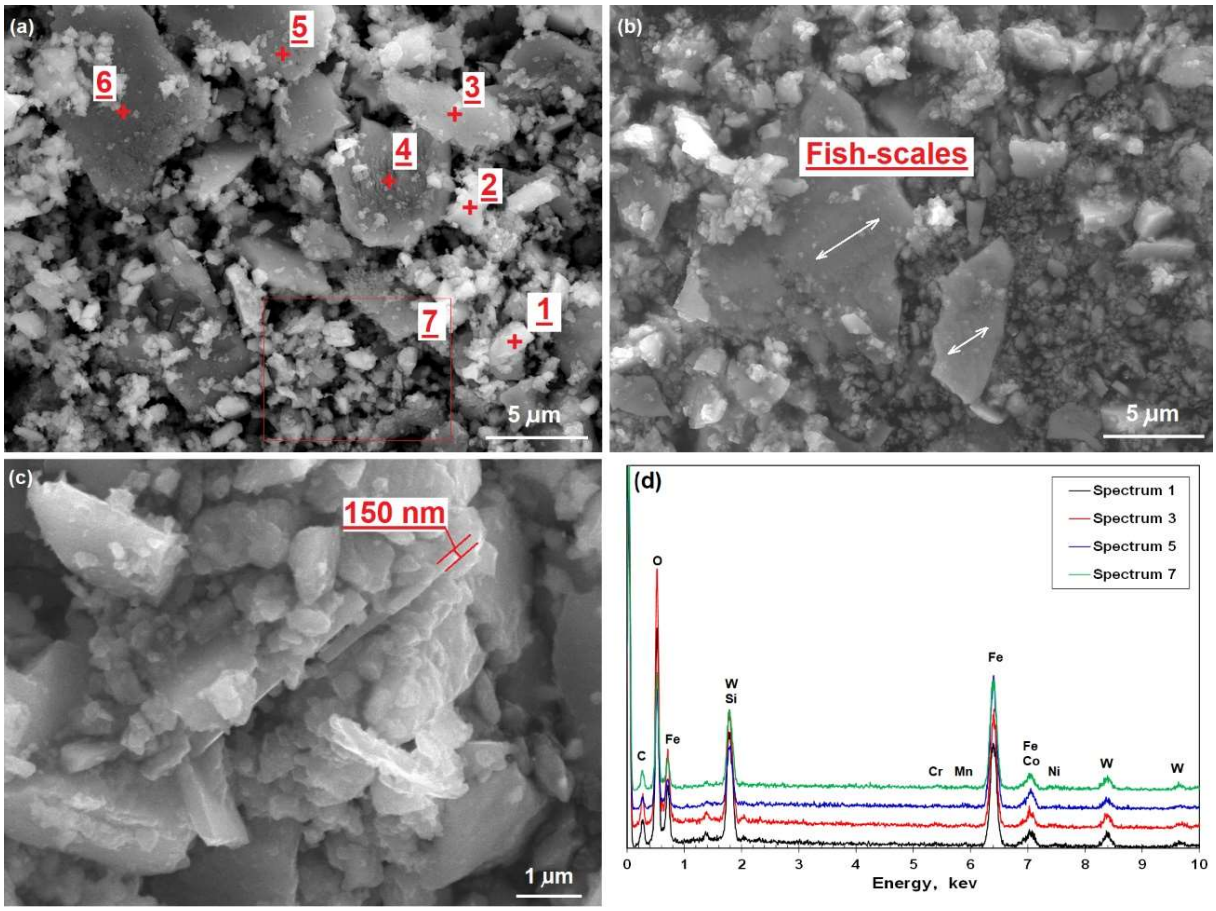

Figure 10 SEM images showing typical morphology of wear debris and the worn surface of the WC counterpart: the wear debris generated after (a) 40 minutes and (b-c) 400 minutes of wear of Sample BM-20; (d) an example EDX spectrum of the wear debris (Spectrum 4).

Table 3 EDX determined chemical compositions (at%) of wear debris as marked in Figure 10a.

Locations	O	Fe	Si	Mn	Cr	Ni	W	Co
1	71.4	21.7	0.0	0.3	0.2	0.5	4.9	1.2
3	73.3	20.7	0.0	0.2	0.2	0.4	4.4	0.8
5	55.5	37.8	0.2	0.3	0.3	0.5	4.2	1.2
7	58.1	33.7	0.1	0.3	0.4	0.5	5.4	1.4

provided evidence to explain the strengthening mechanisms. Thirdly, comparing to conventional quenching treatment, the short-term austempering promoted retention of slightly more austenite, whereas the increased austenite enabled the steel with TRIP effect [29]. Finally, unlike the extra-long austempering time in most reported nano-bainite processes, the new heat treatment reported in this paper only introduced a very short austempering treatment prior to quenching. The short treatment time facilitates cost effective production.

The new austempering treatment has shown the lowest wear coefficient in all the hardened conditions. By applying 20 minutes of austempering at the Ms temperature of 285°C, the wear coefficient has been lowered by 48%, 16% and 26% compared to the as-quenched martensite, tempered martensite and lower bainite, respectively. Combining the findings of wear mechanism study, we believe that the new treatment is able to improve the resistance of wear under severe plastic deformation and spalling, such as in those present in industrial practice [1-4].

Both the martensite and nano-bainite contributed to the improved wear resistance according to the reported finding of microstructure evolution underneath the worn surface. At the depth of approximately 12 µm, shear deformation initiated which can be seen as a transition from elastic straining to plastic straining. The martensite provided strong resistance to shear deformation as its role in the Vickers indentation. Consequently, it slowed the elastic-to-plastic transition, which

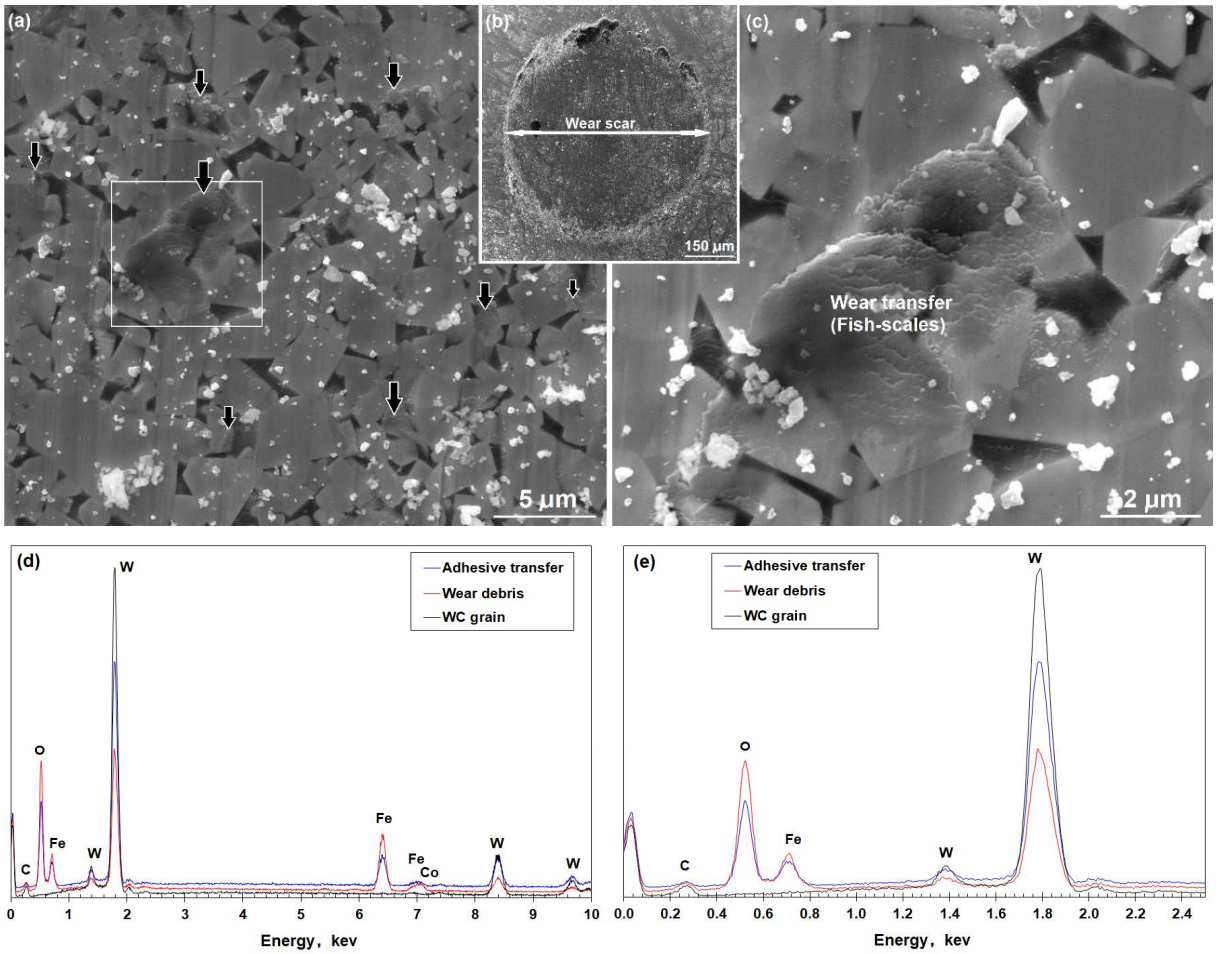

Figure 11 SEM observations and EDX analysis of a typical worn surface of the counterpart WC ball (after 40 minutes of wear of Sample BM-20): (a) the WC worn surface; (b) the whole size of wear scar; and (c) a high-magnification view of the area highlighted in (a) showing fish-scale features attached on the smooth worn surface; and (d-e) EDX spectroscopic analysis of typical areas.

resulted in the lower wear coefficients of the BM-6 and BM-20 than that of the BM-60, Figure 2. Furthermore, the high hardness of the BM-20 sample resulted in the lower wear coefficient, when compared to the lower hardness LB sample.

With the progressive accumulation of plastic strain, the microstructure, approaching the worn surface, underwent extreme evolution through the formation of a microscale band of nano-laminates, Figures 7 and 9. The bainite component, especially the filmy austenite, was able to undergo more plastic straining and strain-hardening than martensite before being embrittled to such a scale to trigger cracking. In other words, the mixture of nano-BF and filmy austenite helped expand the straining hardening capacity as suggested in literature [10, 16, 30, 31]. This explanation is also applied to the lower wear of Sample TM than Sample M, i.e. improved wear resistance by applying a low-temperature tempering to the as-quenched martensite, for the latter is known to be more brittle than the former. We found that the nano-laminates exhibited strong brittleness and compressive residual stresses as featured by the indenting induced cracking and spalling, (seeing Figure 6). Delamination wear failure took place exactly inside this extremely deformed layer. The formation of hard but brittle nano-laminates can be considered as the upper limit of the strain-hardening capacity. Severe plastic deformation is known to generate residual compressive stresses. Although we were not able to measure the stresses because of the small worn surface area, such residual compressive stresses were already measured by other researchers, e.g. on the dry sliding worn surfaces of high strength steel AISI 4340 (-800 MPa) and on the rolling contact zone of rail surfaces (-600 MPa) [32-33].

5 Conclusions

1) Short-term austempering treatment of medium-carbon multi-alloyed steel at its Ms temperature facilitated the formation of refined multi-phase microstructure comprising nano-width bainitic ferrite laths, inter-lath filmy austenite and mixed martensite and retained austenite. The amount and carbon content of retained austenite both increase with increasing austempering time.

2) The short-term austempered samples retained its hardness comparable to, or slightly lower than, the as-quenched martensitic sample. Comparing to the latter, the short-term austempering treatment was able to reduce the wear coefficient by 48% in the applied high-stress sliding wear.

3) The 20 minute austempered sample outperformed the samples conventionally hardened by quenching-tempering and by lower bainite austempering, by 16% and 26% respectively.

4) Adhesive sliding, oxidation and severe plastic deformation were found in the wear of the heat treated steel. Electron microscopic observations of the wear debris, worn surface and subsurface microstructure evolution confirmed that the applied sliding wear brought about the formation of gradient microstructure from progressively increased shear deformation to a nano-laminate top worn surface layer. The nano-laminate structured worn surface became highly stressed and embrittled to trigger cracking and delamination wear failure.

References

[1] S. Sharma, S. Sangal, K. Mondal, Wear behaviour of bainitic rail and wheel steels, Mater. Sci. Technol. 32 (2016) 266-274.

[2] L. K. Lin, Y. M. Xia, Q. S. Mao, X. H. Zhang, Experimental study on wear behaviours of TBM disc cutter ring in hard rock conditions, Tribo. Trans. 61 (2018) 920-929.

[3] K. Valtonen, K. Keltamaki, V.T. Kuokkala, High-stress abrasion of wear resistant steels in the cutting edges of loader buckets, Tribo. Int. 119 (2018) 707-720.

[4] E Abbasi, Q. Luo, D. Owens, Case study: wear mechanisms of NiCrVMo-steel and CrB-steel scrap shear blades, Wear 398-399 (2018) 29-40.

[5] N. P. Suh, The delamination theory of wear, Wear 25 (1973) 111-124.

[6] C. Greiner, Z. Liu, R. Schneider, L. Pastewka, P. Gumbsch, The origin of surface microstructure evolution in sliding friction, Scr. Mater. 153 (2018) 63-67.

[7] C. H. Yin, Y. L. Liang, Y. Jiang, M. Yang, S. L. Long, Formation of nano-laminated structures in a dry sliding wear induced layer under different wear mechanisms of 20CrNi2Mo steel, Appl. Surf. Sci. 423 (2017) 305-313.

[8] Y. D. Chen, R. M. Ren, X. J. Zhao, C. H. Chen, R. Pan, Study on the surface microstructure evolution and wear property of bainitic rail steel under dry sliding wear, Wear 448 (2020) No. 203217.

[9] S. X. Li, Y. S. Su, X. D. Shu, J. J. Chen, Microstructural evolution in bearing steel under rolling contact fatigue, Wear 380-381 (2017) 146-153.

[10] S. Sharma, S. Sangal, K. Mondal, Influence of subsurface structure on the linear reciprocating sliding wear behaviour of steels with different microstructures, Metall. Mater. Trans. 45A (2014) 6088-6102.

[11] J. Speer, D. K. Matlock, B. C. DeCooman, J. G. Schroth, Carbon partitioning into austenite after martensite transformation, Acta Mater. 51 (2003) 2611-2622.

[12] C. Wang, X. Li, Y. Chang, S. Han, H. Dong, Comparison of three-body impact abrasive wear behaviours for quenching-partitioning-tempering and quenching-tempering 20Si2Mi3 steels, Wear 362-363 (2016) 121-128.

[13] F. Hu, K. M. Wu, P. D. Hodgson, Effect of retained austenite on wear resistance of nanostructured dual phase steel, Mater. Sci. Technol. 32 (2016) 40-48.

[14] J. Yang, Y. Jiang, J. Gu, Z. Guo, H. Chen, Effect of austenization temperature on the dry sliding wear properties of a medium carbon quenching and partitioning steel, Acta Metall. Sin. 54 (2018) 21-30.

[15] W. Liu, Y. Jiang, H. Guo, Y. Zhang, A. Zhao, Y. Huang, Mechanical properties and wear resistance of ultrafine bainitic steel under low austempering temperature, Int. J. Miner. Metall. Mater. 27 (2020) 483-493.

[16] B. Narayanaswamy, P. Hodgson, I. Timokhina, H. Beladi, The impact of retained austenite characteristics on the two-body abrasive wear behaviour of ultrahigh strength bainitic steels, Metall. Mater. Trans. A47 (2016) 4883-4895.

[17] Q. Luo, M. Kitchen, S. Abubakri, Effect of austempering time on the microstructure and carbon partitioning of ultrahigh strength steel 56NiCrMoV7, Metals 7 (2017) No. 258.

[18] C. H. Young, H K. D. H. Bhadeshia, Strength of mixtures of bainite and martensite, Mater. Sci. Technol. 10 (1994) 209-214.

[19] Y. Tomita, T. Okawa, Effect of modified heat treatment on mechanical properties of 300M steel, Mater. Sci. Technol. 11 (1995) 245-251.

[20] Q. Luo, Electron microscopy and spectroscopy in the analysis of friction and wear mechanisms, Lubricants 6 (2018) No. 58.

[21] K. T. Park, H. J. Kwon, Interpretation of the strengthening of steel with lower bainite and martensite mixed microstructure, Metals Mater. Int. 7 (2001) 95-99.

[22] M. K. Kang, Y. Q. Yang, Q. M. Wei, Q. M. Yang, X. K. Meng, On the prebainitic phenomenon in some alloys, Metall. Mater. Trans. 25A (1994) 1941-1946.

[23] Z. G. Yang, H. S. Fang, An overview on bainite formation in steels, Curr. Opin. Solid. State. Mater. 9, 2005, 277-286.

[24] Y. Tomita, Development of fracture toughness of ultrahigh strength, medium carbon, low alloy steels for aerospace applications, Int. Mater. Rev. 45 (2000) 27-37.

[25] Y. G. Cao, C. H. Yin, Y. L. Liang, S. H. Tang, Lowering the coefficient of martensitic steel by forming a self-lubricating layer in dry sliding wear, Mater. Res. Express 6 (2019) No 055024.

[26] D. A. Rigney, Transfer, mixing and associated chemical and mechanical processes during the sliding of ductile materials, Wear 245 (2000) 1-9.

[27] Q. Luo, Origin of friction in running-in sliding wear of nitride coatings, Tribo. Lett. 37 (2010) 529-539.

[28] I A. Inman, S. Datta, H. L. Du, J. S. Burnell-Gray and Q. Luo, Microscopy of glazed layers formed during high temperature sliding wear, Wear 254 (2003) 461–467.

[29] L. Liu, B. He, M. Huang, The Role of transformation induced plasticity in the development of advanced high strength steels, Advanced Engineering Materials 20 (2018) No 1701083.

[30] S. M. Hasan, A. Mandal, S. B. Singh, D. Chakrabarti, Work hardening behaviour and damage mechanisms in carbide-free bainitic steel during uni-axial tensile deformation, Mater. Sci. Eng. A 751 (2019) 142-153.

[31] P. V. Moghaddam, J. Hardell, E. Vuorinen, B. Prakash, The role of retained austenite in dry rolling/sliding wear of nanostructured carbide-free bainitic steel, 428-429 (2019) 193-204.

[32] J. W. Ho, C. Noyan, J. B. Cohen, Residual stresses and sliding wear, Wear 84 (1983) 183-202.

[33] A Pyzalla, L. Wang, E. Wild, T. Wroblewski, Changes in microstructure, texture and residual stresses on the surface of a rail resulting from friction and wear, Wear 251 (2002) 901-907.